# Dalton Transactions

Accepted Manuscript

This is an *Accepted Manuscript*, which has been through the Royal Society of Chemistry peer review process and has been accepted for publication.

*Accepted Manuscripts* are published online shortly after acceptance, before technical editing, formatting and proof reading. Using this free service, authors can make their results available to the community, in citable form, before we publish the edited article. We will replace this *Accepted Manuscript* with the edited and formatted *Advance Article* as soon as it is available.

You can find more information about *Accepted Manuscripts* in the Information for Authors.

Please note that technical editing may introduce minor changes to the text and/or graphics, which may alter content. The journal's standard Terms & Conditions and the Ethical guidelines still apply. In no event shall the Royal Society of Chemistry be held responsible for any errors or omissions in this *Accepted Manuscript* or any consequences arising from the use of any information it contains.

ROYAL SOCIETY OF CHEMISTRY

www.rsc.org/dalton

Dalton Transactions

COMMUNICATION

# EPR detection and characterisation of a paramagnetic Mo(III) dihydride intermediate involved in electrocatalytic hydrogen evolution

Received 00th January 20xx,
Accepted 00th January 20xx

DOI: 10.1039/x0xx00000x

www.rsc.org/

Christopher Prior,[a] Lee R. Webster,[a] Saad K. Ibrahim,[a] Joseph A. Wright, [a] Ali F. Alghamdi, [a] Vasily S. Oganesyan*[a] and Christopher J. Pickett*[a]

**EPR spectroscopy and theoretical data show that the slow heterogeneous electron-transfer kinetics associated with the reduction of an 18-electron Mo(IV) acetato dihydride are a consequence of an $\eta^2$–$\eta^1$ rearrangement of the carboxylate ligand which gives a unique paramagnetic *17-electron* Mo(III) dihydride.**

The $\{M(Ph_2PCH_2CH_2Ph_2)_2\}$ platform, where M = Mo or W and related 1,2-bis(tertiary diphospho)alkane complexes, supports a diverse range of ligand centred chemistry and electrochemistry. This includes protonation of dinitrogen, nitrido, isocyanide and nitrile ligands,[1,2,3] oxidation of methyleneamido ligands to cyanide,[4] reduction of cyanide to the aminocarbyne ligand [5], N-N cleavage of dialkylhydrazides,[6] and electrosynthetic pathways to ammonia, amines and aminoacids.[7,8,9] Such platforms also support electrocatalytic hydrogen evolution, for example, the carboxylato-complexes $[MH_2(\eta^2\text{-RCOO})(Ph_2PCH_2CH_2PPh_2)_2]^+$ **A**$^+$ (M = Mo; R = alkyl) first reported by Ito and coworkers [10] have been shown to electrocatalyse the reduction of protons to dihydrogen at modest turnover frequencies,[9,11] and this has been extended to photoelectrocatalysis at semiconductor electrodes.[12] Central to the proposed mechanism for hydrogen evolution, and also to chemistry which leads to the binding of molecular nitrogen or other ligands, is the invocation of a paramagnetic intermediate $[MH_2(\eta^1\text{-MeCOO})(Ph_2PCH_2CH_2PPh_2)_2]$ **A**$^o$ where the $\eta^2$-carboxylate of the parent complex has opened to give an $\eta^1$-ligand, following slow electron-transfer.

Hitherto, only *indirect* experimental evidence has provided support for this rearrangement. Specifically (i) the observation by cyclic voltammetry of a *quasi-reversible* one-electron reduction whereby the slow heterogenous kinetics have been taken to signal inner sphere reorganisation concerted with the electron-transfer [11], and (ii) the isolation and X-ray crystallographic characterisation of a stable trihydride $[MH_3(\eta^1\text{-MeCOO})(Ph_2PCH_2CH_2PPh_2)_2]$ (M = W) The crystallographic structure of which shows that the carboxylate has an $\eta^1$ coordination mode, Scheme 1 [13,14]. This intramolecularly hydrogen-bonded trihydride is formed by 'trapping' **A**$^o$ (M = W; R = Me) by a further one electron reduction and protonation, Scheme 1. We now report the detection by EPR (electron paramagnetic resonance) spectroscopy of the key paramagnetic Mo(III) dihydride intermediate **A**$^o$ (M = Mo, R = Me) and its dideuteride analogue, Scheme 1. The fitting of the EPR spectra in combination with rigorous quantum mechanical modelling of the observed spectral features, now provide compelling evidence in support for the 'open' carboxylate $\eta^1$-coordination mode in **A**$^o$, as originally postulated.[11] Syntheses and characterisation of the new complexes used in this study together with crystallographic data for **A**$^+$ (M = Mo, W; R = H) are given in the Supplementary Information (SI).

We first establish the generic *quasi*-reversible behaviour of the **A**$^{+/o}$ carboxylate couples. The sets of cyclic voltammograms shown in Figure 1 were recorded at a vitreous carbon electrode in the solvent system $[NBu_4][BF_4]^-$ toluene 1:3 at 303 K, a solvent of low reactivity

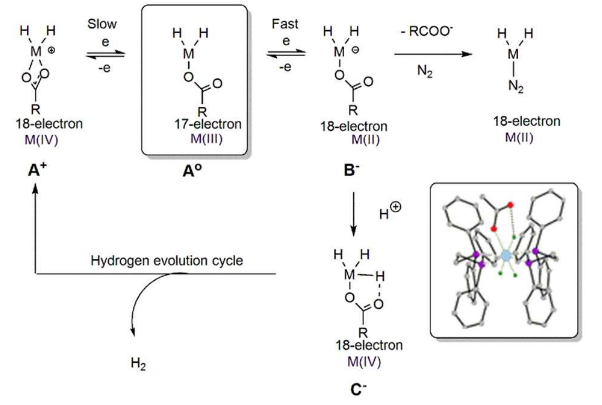

**Scheme 1.** Summary of electron-transfer chemistry of $[MH_2(\eta^2\text{-MeCOO})(Ph_2PCH_2CH_2PPh_2)_2]^+$ **A**$^+$ together with a view of the reported structure of the isolated tungsten trihydride **C** showing the 'open' carboxylate form, see ref 13.

---

[a] *Energy Materials Laboratory, School of Chemistry, University of East Anglia, Norwich Research Park, Norwich NR4 7TJ, UK.*

Electronic Supplementary Information (ESI) available: Synthesis of $[MH_2(O_2CR)(dppe)_2][BPh_4]$ complexes, spectroscopic characterisation & crystal data, electrochemical and EPR measurements and simulations, DFT computational details. See DOI: 10.1039/x0xx00000x

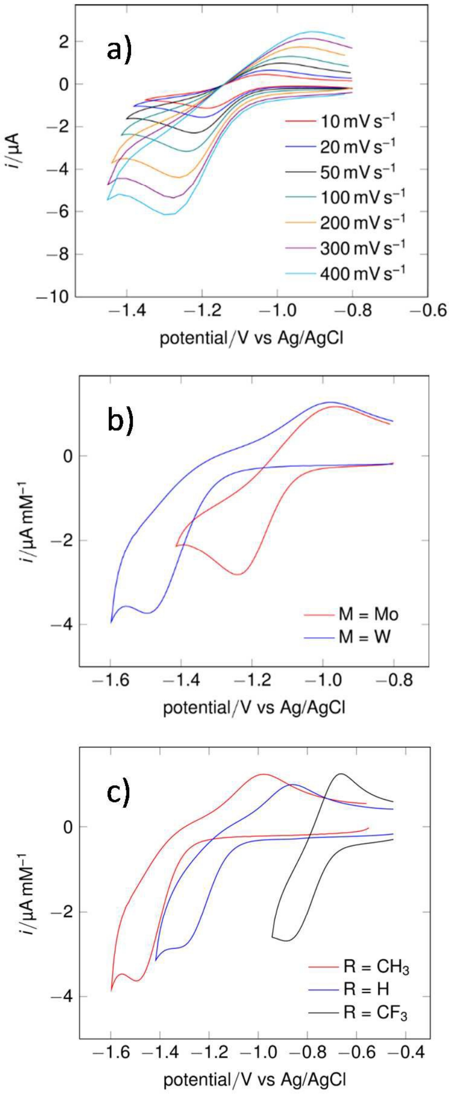

**Figure 1**. Cyclic voltammograms for the $[MH_2(\eta^2\text{-}RCOO)(Ph_2PCH_2CH_2PPh_2)]^+$ complexes recorded at 303 K at a vitreous carbon electrode, area 0.071 cm$^2$, in $[NBu_4][BF_4]$-toluene 1:3 molar ratio. a) Scan rate dependence for M = Mo; R = Me b) Complexes M = Mo and W; R = Me at 100 mV s$^{-1}$ c) Complexes M = W; R = Me, H and $CF_3$ at 100 mV s$^{-1}$.

in which both redox partners are stable.[15] As is fully consistent with slow heterogenous electron–transfer kinetics, the magnitude of the peak separation Δ*E* for the $\mathbf{A}^{+/o}$ (M = Mo, R =Me) couple increases with increasing scan-rate as is illustrated in Figure 1(a). From this data the standard heterogenous electron-transfer rate constant[16] was determined by digital simulation[17] to be $k_o^{Mo,Me}$ = (1.0 ± 0.1) × $10^{-4}$ cm s$^{-1}$ at 303 K. Corresponding values for the 'fast' reversible ferrocene-ferrocinium couple where solvent reorganisation dominates the heterogenous electron transfer kinetics are typically more than three orders of magnitude faster.[18] The nature of the metal centre influences the electron-transfer kinetics, Figure 1(b). Thus the electron-transfer rate constant for the tungsten complex under measured under identical conditions, $k_o^{W,Me}$ = (0.2 ± 0.02) × $10^{-4}$ cm s$^{-1}$ , is about a factor of 5 slower than that for the Mo analogue. This can be attributed to strength of the $M{-}O_{acetate}$ bonds which are expected to be greater for W than for Mo. Figure 1(c) shows a comparison of the voltammograms for complexes $[MH_2(\eta^2\text{-}RCOO)(Ph_2PCH_2CH_2PPh_2)_2]^+$ (M = W; R = Me, H and $CF_3$ ). The inductive influence of the carboxylate substituent R clearly has an effect on the magnitude of the formal potential $E^{o'}$: the W complex with the more electron-withdrawing R = $CF_3$ group is 510 ± 10 mV easier to reduce than is its R = Me analogue. There is also a substantial effect of the substituent group on the electron-transfer kinetics, $k_o^{W,CF3}$ is about order of magnitude greater than $k_o^{W,Me}$ , consistent with a weaker W−O bond and greater lability in the R = $CF_3$ complex. Heterogenous electron-transfer rate constants for these systems together with parameters used in the simulations are tabulated in the SI.

The reduction of the dihydride $\mathbf{A}^+$ (M = Mo; R = Me) was carried out in the cavity of an EPR spectrometer by controlled-potential electrolysis at a platinum wire working electrode in tetrahydrofuran containing 0.2 M $[NBu_4][BF_4]$ as the supporting electrolyte under an atmosphere of argon. The potential was set at the onset of reduction of the complex. The room temperature EPR spectra obtained by reduction of both $\mathbf{A}^+$ (M = Mo, R = Me) and its $^2$H analogue are shown as black lines in Figures 2 a) and b), respectively. There is a

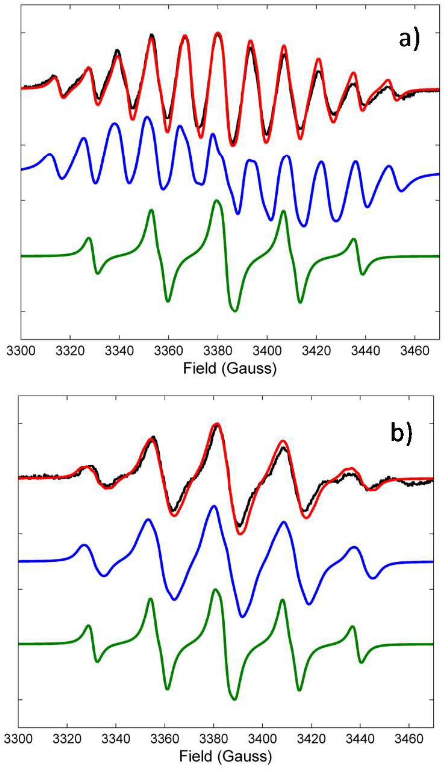

**Figure 2**. EPR spectra of $\mathbf{A}^o$ (a) and its deuterated form (b). In each panel black,red and blue lines correspond to experimental, fitted and predicted from DFT spectra, respectively. Spectra obtained with hydrogen and deuterium

hyperfine couplings excluded from the EPR simulation are shown by green lines.

considerable difference between their EPR lineshapes. Both spectra were fitted using the fast motional regime model as implemented in Easyspin software [19] and the adjusted parameters are summarized in Table 1.

Analysis reveals that the EPR spectra result from large hyperfine coupling to four phosphorous nuclei in a 1:4:6:4:1 pattern, with further splitting from the hydrides in a 1:2:1 pattern. Since the isotropic coupling constants of phosphorous is about twice that of the hydrides, in **A**$^{o}$ the internal lines from the hydride splitting overlay giving eleven discernible lines instead of fifteen. Upon deuteration, the hydrogen splitting is reduced by the magnetogyric ratio, $\gamma_D/\gamma_{H,}$ ($A_{Iso}(^1H)= -39.1$ Mhz/ $A_{Iso}(^2H)= -7.3$ MHz) to a magnitude where it is not resolved due to line broadening, leaving only the splitting pattern from the phosphorous nuclei. The acetate group has negligible interactions with the spin system. In the simulations the negative signs of the major $A_{Iso}$ ($^{31}P$, H) components were assigned on the basis of a slight increase in linewidth across the spectra, with the low magnetic field $m_I$ =-I line being marginally narrower than that of the high magnetic field $m_I$=+I feature. This was confirmed by an increase in the accuracy of fitting when using negative values as well as the DFT calculations.

EPR measurements indicate that the unpaired electron is essentially located on the metal centre. The effect is particularly noticeable in the extended EPR spectrum of the deuterated form of **A**$^{o}$ where hyperfine splitting from hydrides is reduced. The contributions from Mo to the hyperfine occur from the $Mo^{95}$ (I=5/2, 15.92%) and $Mo^{97}$ (I=5/2, 9.55%) isotopes and result in characteristic low intensity features visible either side of the five lines arising from phosphorous splitting (see Figure S2 of SI). The fitted value of 78 MHz for the hyperfine coupling contribution from Mo is in excellent agreement with previous reports on organodiazenido Mo complexes.[20]

The structure of complex **A**$^{o}$ was optimized using DFT calculations (Gaussian 09 [21]) followed by prediction of magnetic parameters ($A$ and $g$) (Details are provided in SI). The complex was found to be of $C_1$ symmetry, with two phosphorous atoms distorted slightly out of the molecular plane, with opposite positions distorted in the same direction in a two up two down arrangement (Figure 3). The hydrides were slightly rotated away from the linear P-Mo-P axis. Importantly, upon reduction of the complex from 18-electron system (diamagnetic state) to the 17-electron system (paramagnetic state) the orientation of the $COOCH_3$ ligand with respect to Mo changes from fully symmetric (Scheme 1) to one in which a single O atom is bound to Mo with an Mo–O–C angle of ~125°. The core structure of **A**$^{o}$ is presented in Figure 3 with full atomic coordinates provided in SI. Magnetic parameters calculated from DFT are summarized in Table 1 and are compared with the ones obtained from the fitting of EPR spectra. There is a perfect agreement for the $A$ values of both $^1H$ and $^2H$. The distribution of the isotropic phosphorous coupling constants is consistent between the fitted values and DFT, including the signs. As often reported for paramagnetic complexes containing phosphorous atoms, the predicted isotropic $^{31}P$ couplings are underestimated compared to experimental ones.[22]

| Parameter | EPR | DFT $C_1$ |
|---|---|---|
| $g_{iso}$ | 2.016 | 2.039 |
| $A_{iso}$ ($^{31}P$) | -82.2 | -88.83 |
| | -78.9 | -78.05 |
| | -73.0 | -76.05 |
| | -69.2 | -66.19 |
| $A_{iso}$ ($^1H$) | -37.8 | -38.4 |
| | -40.4 | -38.5 |
| $A_{iso}$ ($^2H$) | -7.4 | -6.0 |
| | -7.3 | -6.0 |

**Table 1.** Comparison between magnetic parameters obtained from the fitting of EPR spectra with those predicted from DFT.[23] Isotropic hyperfine coupling constants are given in MHz.

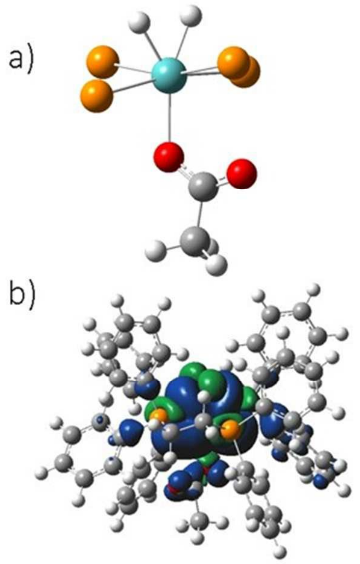

**Figure 3.** DFT optimized structures of $[MoH_2(\eta^1\text{-}CH_3COO)(Ph_2CH_2CH_2Ph_2)_2]^0$ a) Core $\{MoP_4H_2OC{=}OCH_3\}$ arrangement showing deployment of acetate group in $\eta^1$-configuration [orange = P; blue = Mo; white = H ; grey = C] b) Isosurfaces of the spin density distribution of complex **A**$^{o}$. Green and blue show the two phases of the spin-density distribution. Note spin density for the hydrides in the apical positions (green).

Thus a factor of ~1.44, which is in agreement with previous DFT studies of Mo-P complexes,[22] has been used to scale the P hyperfine coupling values. The EPR spectra predicted using the parameters calculated by DFT are shown in Figure 2 as middle (blue) lines in panels a) and b) for **A**$^{o}$ and its $^2H$ analogue, respectively, demonstrating a good agreement with hydrides. The impact of the hydrogen and deuterium hyperfine couplings on the EPR lineshapes can be clearly seen by excluding their relevant contributions from the EPR simulation. The results are presented as green curves in Figure 2 a) and b) for **A**$^{o}$ and its $^2H$ analogue, respectively.

DFT calculations indicate that spin density in all systems is primarily localized on the molybdenum centre (Figure 3), which accounts for 62% of the total unpaired spin density. The P atoms bear a considerable spin density (a total of 12%) and ~1% of the density resides on the nearest to Mo O atom. The hydrides are characterized by large s-orbital spin density (~3.0% per hydride) due to the direct interaction with molybdenum, being roughly equal to the total s orbital spin density of all the phosphorous atoms (calculated with standard isotropic atomic hyperfine coupling values).[24]

Both experimental EPR spectra and DFT calculations lead to a conclusion that two H atoms in complex **A$^{o}$** are ligated to Mo ion and possess strong hyperfine coupling. The Mo-H distance is 1.74 Å and the H-Mo-H angle is ~60° (see Table 2). The results for complex **A$^{o}$** are also consistent with our recent study on a paramagnetic μ-hydride di-iron dithiolate complex with significant hyperfine coupling on the single bridging hydride ($A_{iso}$ ~ −75 MHz)[25]. The values of both $A_{iso}$(P) and $A_{iso}$(H) hyperfine couplings are also consistent with the relevant values reported for a paramagnetic Mo(V) polyhydride complex[26].

| Parameter | DFT |
|---|---|
| Mo–P | 2.47 Å |
| | 2.49 Å |
| | 2.50 Å |
| | 2.49 Å |
| H–H | 1.71 Å |
| Mo–H | 1.74 Å |
| | 1.73 Å |
| H–Mo–H | 59.0° |
| Mo–O | 2.19 Å |
| Mo–O–C | 125.0° |

**Table 2.** Selected structural parameters (distances and angles) of the DFT optimised complex **A$^{o}$**.

Spectroscopic and theoretical data show that the slow heterogeneous electron-transfer kinetics associated with the single electron reduction of the Mo(IV) 18-electron dihydride are now fully explained by a concerted $\eta^2$–$\eta^1$ rearrangement of the carboxylate co-ligand. This gives the 17-electron Mo(III) dihydride intermediate avoiding the formation of a high energy 19-electron species. Paramagnetic molybdenum and tungsten hydrides are rather rare and largely confined to more or less unstable Mo(V) species.[27] Only one example of a Mo(III) hydride species has been spectroscopically characterized, an unstable monohydride reported by Schrock and co-workers,[28] the Mo(III) dihydride detected herein is unique.

We thank Taibah University, Saudi Arabia, for funding Dr Ali Alghamdi to undertake a period of research at the Energy Materials Laboratory. The EPSRC is thanked for providing postgraduate studentship to LRW. The EPSRC is thanked for supporting this work through grants to CJP (EP/H019480/1) and VSO (EP/L001322/1). We gratefully acknowledge the EPSRC UK National Crystallography Service at the University of Southampton for the collection of the crystallographic data.[28]

## Notes and references

1. J. Chatt, J. R. Dilworth and R. L. Richards, *Chem. Rev.*, 1978, **78**, 589-625.
2. R. A. Henderson, G. J. Leigh and C. J. Pickett, *Adv. Inorg. Chem. Radiochem.*, 1983, **27**, 197-292.
3. H. Seino, Y. Mizobe and M. Hidai, *Chem. Rec.*, 2001, **1**, 349-361.
4. A. Hills, D. L. Hughes, C. J. Macdonald, M. Y. Mohammed and C. J. Pickett, *J. Chem. Soc., Dalt. Trans.*, 1991, 121-129.
5. D. L. Hughes, S. K. Ibrahim, H. M. d. Ali and C. J. Pickett, *J. Chem. Soc., Chem. Com.*, 1994, 425-427.
6. R. A. Henderson, G. J. Leigh and C. J. Pickett, *J. Chem. Soc., Dalt. Trans.*, 1989, 425-430.
7. C. J. Pickett, *J. Bio. Inorg. Chem.*, 1996, **1**, 601-606.
8. C. J. Pickett and J. Talarmin, *Nature*, 1985, **317**, 652-653.
9. D. L. Hughes, S. K. Ibrahim, C. J. Macdonald, H. M. Ali and C. J. Pickett, *J. Chem. Soc., Chem. Com.*, 1992, 1762-1763.
10. T. Ito, A. Takahashi and S. Tamura, *Bull. Chem. Soc. Japan.*, 1986, **59**, 3489-3494.
11. D. L. Hughes, S. K. Ibrahim, C. J. Pickett, G. Querne, A. Laouenan, J. Talarmin, A. Queiros and A. Fonseca, *Polyhedron*, 1994, **13**, 3341-3348.
12. L. R. Webster, S. K. Ibrahim, J. A. Wright and C. J. Pickett, *Chem. Eur. J.*, 2012, **18**, 11798-11803.
13. S. A. Fairhurst, R. A. Henderson, D. L. Hughes, S. K. Ibrahim and C. J. Pickett, *J. Chem. Soc., Chem. Com.*, 1995, 1569-1570.
14. R. A. Henderson, S. K. Ibrahim, K. E. Oglieve and C. J. Pickett, *J. Chem. Soc., Chem. Com.*, 1995, DOI: 10.1039/C39950001571, 1571-1572.
15. C. J. Pickett, *J. Chem. Soc., Chem. Com.*, 1985, 323-326.
16. A. D. Clegg, N. V. Rees, O. V. Klymenko, B. A. Coles and R. G. Compton, *J. Electroanal. Chem.*, 2005, **580**, 78-86.
17. M. Rudolph, *Digielch 4.0*, Germany, Elchsoft, 2006.
18. L. Xiao, E. J. F. Dickinson, G. G. Wildgoose and R. G. Compton, *Electroanal.*, 2010, **22**, 269-276.
19. S. Stoll and A. Schweiger, *J. Mag. Res.*, 2006, **178**, 42-55.
20. G. Butler, J. Chatt, G. J. Leigh and C. J. Pickett, *J Chem Soc Dalton*, 1979, 113-116.
21. M. J. Frisch, *et al. Gaussian 09 Revision C01*, Gaussian Inc., Wallingford CT, 2009.
22. H. Sidorenkova, T. Berclaz, B. Ndiaye, A. Jouaiti and M. Geoffroy, *J. Phys. Chem. Solids*, 2009, **70**, 713-718.
23. Since in the fast motional regime the averaged g value has only a systematic shift effect on the EPR spectrum in all simulated spectra its fitted value was employed. b) A scaling factor of 1.44 was applied for the AIso (31P) values predicted from DFT (see text).
24. J. E. Wertz and J. R. Bolton, *Electron spin resonance : elementary theory and practical applications*, McGraw-Hill, New York ;, 1972.
25. A. Jablonskyte, J. A. Wright, S. A. Fairhurst, J. N. T. Peck, S. K. Ibrahim, V. S. Oganesyan and C. J. Pickett, *J. Am. Chem. Soc.*, 2011, **133**, 18606-18609.
26. D. L. Hughes, D. J. Lowe, M. Y. Mohammed, C. J. Pickett and N. M. Pinhal, *J. Chem. Soc. Dalton Trans.*, 1990, 2021-2027.
27. B. Pleune, D. Morales, R. Meunier-Prest, P. Richard, E. Collange, J. C. Fettinger and R. Poli, *J. Am. Chem. Soc.*, 1999, **121**, 2209-2225.

28. R. A. Kinney, D. G. H. Hetterscheid, B. S. Hanna, R. R. Schrock and B. M. Hoffman, *Inorg. Chem.*, 2010, **49**, 704-713.